Articles in PresS. J Neurophysiol (August 3, 2011). doi:10.1152/jn.00496.2011

The Roles of Conserved and Non-Conserved Cysteinyl Residues in the Oligomerization and Function of Mammalian Prestin

Benjamin Currall, Danielle Rossino, Heather Jensen-Smith, Richard Hallworth

Department of Biomedical Sciences, Creighton University School of Medicine, Omaha, Nebraska 68178

Running Head: Conserved and Non-Conserved Cysteinyl Residues in Prestin

Corresponding Author:
Richard Hallworth
Department of Biomedical Sciences
Creighton University
2500 California Plaza
Omaha, Nebraska 68178
USA
Phone: 402 280-3057
FAX: 402 280-2690
Email: hallw@creighton.edu

Abstract

The creation of several prestin knock-out and knock-in mouse lines has demonstrated the importance of the intrinsic outer hair cell membrane protein prestin to mammalian hearing. However, the structure of prestin remains largely unknown, with even its major features in dispute. Several studies have suggested that prestin forms homo-oligomers that may be stabilized by disulfide bonds. Our phylogenetic analysis of prestin sequences across chordate classes suggested that the cysteinyl residues could be divided into three groups, depending on the extent of their conservation between prestin orthologs and paralogs or homologs. An alanine scan functional analysis was performed of all nine cysteinyl positions in mammalian prestin. Prestin function was assayed by measurement of prestin-associated non-linear capacitance. Of the nine cysteine-alanine substitution mutations, all were properly membrane-targeted and all demonstrated non-linear capacitance. Four mutations (C124A, C192A, C260A, and C415A), all in non-conserved cysteinyl residues, significantly differed in their non-linear capacitance properties compared to wild-type prestin. In the two most severely-disrupted mutations, substitution of the polar residue seryl for cysteinyl restored normal function in one (C415S) but not the other (C124S). We assessed the relationship of prestin oligomerization to cysteine position using FRET. With one exception, cysteine-alanine substitutions did not significantly alter prestin-prestin interactions. The exception was C415A, one of the two non-conserved cysteinyl residues whose mutation to alanine caused the most disruption in function. We suggest that no disulfide bond is essential for prestin function. However, C415 likely participates by hydrogen bonding in both in non-linear capacitance and oligomerization.

Keywords: hair cell, hearing, molecular motor, disulfide bond, FRET

Introduction

The cochlear outer hair cell motor protein prestin is thought to play a major role in mammalian cochlear amplification (Dallos 2008). Prestin is thought to participate in the generation of mechanical energy in the cochlea by means of receptor potential-driven outer hair cell (OHC) length change. The creation of several prestin knock-out and knock-in mouse lines with hearing-loss phenotypes has convincingly demonstrated the importance of prestin to mammalian hearing (Dallos et al. 2008; Liberman et al. 2002).

Associated with the length change of OHCs is non-linear capacitance (NLC), which can also be detected when prestin is expressed in a cell line such as HEK 293 cells, or opossum kidney cells (Ludwig et al. 2001; Zheng et al. 2000). Briefly, NLC refers to the asymmetric charging properties of prestin-containing cellular membranes (Iwasa 1993; Santos-Sacchi 1991). In isolated OHCs, NLC and force generation have proved nearly inseparable. Although deflation of the OHC eliminates length change without also eliminating NLC (Kakehata and Santos-Sacchi 1995), no procedure has yet been shown to block NLC without also blocking OHC length change. Thus NLC serves as a proxy measure of prestin function. NLC is also found in non-placental mammal prestins in expression systems (Tan et al. 2010) and electromotility has also been observed in marsupial OHCs (Okoruwa et al. (2008) and our own observations)

Prestin is a trans-membrane protein of 744 residues in mammals and is a member of an anion transporting protein family, the solute carrier 26, or Slc26a, family (prestin is Slc26a5) (Zheng et al. 2000). The other members of the Slc26 family, where known, are transporters of various species of anion (Dorwart et al. 2008; Ohana et al. 2009). Prestin apparently does not transport anions, although it does require the anion chloride for its conformation change and for NLC (Oliver et al. 2001), which may be a relic of a former transporter identity. Consistent with

this hypothesis, the non-mammalian prestin homologs from *G gallus* and *D. rerio* are divalent anion exchangers (Schaechinger and Oliver 2007).

The region, domain, and motif structure of mammalian prestin is shown in Fig. 1A. Of particular importance to our analysis are the sulfate transporter (SulP) and the carboxy-terminal STAS (Sulfate Transporter and anti-Sigma factor antagonist) domain (Ohana et al. 2009). These features are common to nearly all Slc26a5 homologs. Prestin also forms homo-oligomers of unknown stoichiometry, as has been consistently shown by Western blot analysis (Zheng et al. 2006) and fluorescence resonance energy transfer (FRET) analysis (Greeson et al. 2006; Navaratnam et al. 2005; Wu et al. 2007). There is evidence that oligomerization is a common feature of Slc26 family proteins (Detro-Dassen et al. 2008).

A cysteinyl residue in a polypeptide may contribute to tertiary structure by forming disulphide bonds, either within the polypeptide or between polypeptide strands in oligomers. Cysteinyl residues may also contribute hydrogen bonding to tertiary structure by virtue of their polar character. The mammalian prestin sequence includes 9 cysteinyl residues. Their positions in the two published structures are shown in Fig. 2. Two of the positions are consensus intracellular (C52 and C679) and are therefore readily accessible for inter- or intra-molecular sulfhydryl linkages. A third, C260, may or may not be included in the membrane. The other six are thought to be in membrane-spanning regions, although this would not completely preclude their participation in sulfhydryl linkages.

We first examined the evolutionary conservation of cysteinyl residues in prestin and related proteins in mammals and non-mammals. We determined which cysteinyl residues were conserved, either in identity, which may signify the requirement for a sulfhydryl linkage, or in similarity, which may indicate that the polar character of the residue is important.

We then performed an alanine scan functional analysis of the nine cysteinyl residues in gerbil prestin. NLC was measured in HEK 293 cells transfected with plasmids expressing mutated prestins and wild-type. Cysteinyl residues were singly mutated to alanyl residues by site-directed mutagenesis. Each sequence was conjugated at its carboxy-terminal with enhanced GFP (eGFP) to indicate which cells were synthesizing prestin. Substitution of alanine at a position occupied by a cysteine eliminated both sulfhydryl bonding and any hydrogen bonding essential to function. For those mutations in which a large functional effect was observed, we then back-substituted the similarly-sized polar residue seryl to distinguish between polar and sulfhydryl contributions of the original cysteinyl.

We next determined the importance of each residue to prestin oligomerization by fluorescence resonance energy transfer (FRET) analysis. In FRET, the energy conferred to a donor fluorophore by a photon in its excitation wavelength range is partly transferred by non-radiative mechanisms to an acceptor fluorophore, from which a photon is emitted in the acceptor's emission wavelength range. FRET occurs only if the donor and acceptor fluorophores are within molecular dimensions of each other, and thus the presence of FRET may be taken as an indication of association. In previous studies, prestin was coupled at its carboxy-terminal to the fluorescent proteins CFP (cyan fluorescent protein) or Venus YFP (Venus yellow fluorescent protein, or vYFP) (Greeson et al. 2006; Navaratnam et al. 2005; Wu et al. 2007). In this study, we used the monomeric Teal blue fluorescent protein variant (mTFP), which was chosen because it does not bind to itself or other fluorescent proteins (Day et al. 2008). We measured FRET using the acceptor photobleach technique and fluorescence lifetime imaging, which have been demonstrated to yield more reliable results than intensity-based methods (Suhling et al. 2005).

Materials and Methods

Sequence Comparison. The *Homo sapiens* prestin sequence (NP_945350.1) was used to retrieve prestin homologs from evolutionarily-relevant using the Basic Local Alignment Search Tool (BLAST) through NCBI (www.blast.ncbi.nlm.nih.gov). Retrieved sequences were aligned using the CLC Main Workbench custom alignment algorithm (CLC Bio, Cambridge, MA) with default parameters (Feng and Doolittle 1987). Aligned sequences with large gaps or insertions (> 50 residues) were rejected. Phylogeny analysis was also performed with CLC Main Workbench using the Unweighted Pair Group Method with Arithmetic Mean with 100 bootstrap replicates.

Plasmid Constructs. For the NLC studies, a plasmid containing gerbil prestin cDNA, ligated in frame to enhanced GFP (eGFP) cDNA (here referred to as pgPG) was obtained from Dr. Peter Dallos (Northwestern University, Evanston, Illinois). Cysteine-substitution mutations were performed using the QuickChange® II Site-Directed Mutagenesis Kit (Agilent, Santa Clara, CA) according to manufacturer's instructions. Correct sequence was confirmed by analysis of the insert performed at the Creighton University Molecular Biology Core Laboratory.

For the FRET studies, the pmTFP1-C construct containing the cDNA for the donor monomeric Teal fluorescent protein (mTFP) was obtained from Allele Biotechnology (San Diego, CA). The Venus construct, which contained the cDNA for the acceptor Venus yellow fluorescent protein (vYFP), was obtained from Dr. Atsushi Miyawaki (RIKEN Brain Science Institute, Saitama, Japan) (Nagai et al. 2002). Using PCR cloning, the mTFP and vYFP cDNA were cloned into the pAcGFP-N1 plasmid construct, replacing the cDNA for *Aequorea coerulescens* green fluorescent protein (GFP), to create the pmTFP-N1 and pvYFP-N1 constructs. Gerbil prestin cDNA, without the stop codon, was PCR-cloned in-frame to the pmTFP-N1 and pvPYFP-N1 constructs 5' to the fluorescent protein open reading frame.

Cysteine-substitution mutations for all constructs were performed using the QuickChange II site-directed mutagenesis kit (Agilent Technologies, Santa Clara, CA) according to the manufacturer's instructions. Correct sequence was confirmed by sequence analysis of the insert performed at the Creighton University Molecular Biology Core Facility.

Two other constructs, as FRET positive and negative controls, were obtained as plasmids from Dr. Jian Zuo. The positive control consisted of a plasmid expressing a construct of Cerulean and Venus fluorescent proteins linked by a short amino acid sequence (here referred to as pLink). The negative control consisted of a construct of the unrelated SLC family protein SLC38A2, linked C-terminal to Venus fluorescent protein (here referred to as p38Y). Both plasmids have previously been used as controls in this laboratory (Wu et al. 2007).

Cell Culture. Human embryonic kidney (HEK 293) cells were obtained from the American Type Culture Collection and were grown in flasks or on 35 mm glass-bottomed dishes by standard methods, without antibiotics.

Transfection. HEK 293 cells were transfected with plasmid(s) when plated cells reached between 80-100% confluency using Lipofectamine™ 2000 by following the manufacturer's protocol (Invitrogen, Carlsbad, CA). For NLC measurements, cells were examined 24-48 hr after transfection. In one experimental series (C415S), 10 μM salicylate was added to the medium to promote translocation to the plasma membrane (Kumano et al. 2010). Salicylate blocks prestin NLC, so the salicylate was removed at least one hour before electrophysiological measures (Kakehata and Santos-Sacchi 1996; Tunstall et al. 1995).

For co-transfection and FRET experiments, if donor and acceptor fluorescence intensity were not approximately equal, plasmid volumes were adjusted to compensate. Cells were fixed between 24-48 hours after transfection using 4% paraformaldehyde in phosphate-buffered saline

(PBS). After 30 minutes fixation, cells were washed with PBS and mounting medium was applied (1:1 v-v PBS: glycerol). Coverslips (#1½ 30 mm round, Warner Instruments, Hamden, CT) were sealed over the cells using rubber cement (Elmer's Products Inc., Columbus, OH). Plates were stored at 4˚C in the dark prior to experimentation.

Determination of Membrane Targeting. The incubation medium surrounding transfected HEK cells was removed and replaced with PBS containing 2 μg/ml wheat germ agglutinin coupled to the red fluorophore Alexa Fluor 568 (WGA-568: Invitrogen). After 10 min exposure to WGA-568, the cells were rinsed three times with PBS alone, and fixed using 4% paraformaldehyde in PBS (30 min). The fixed cells were rinsed in PBS, mounted in mounting medium, and cover-slipped and sealed as described above. Cells were examined using the LSM 510 META NLO confocal microscope (Carl Zeiss Inc., Thornwood, NY) of the Creighton University Integrated Biomedical Imaging Facility (IBIF). Images were analyzed using ImageJ (http://rsbweb.nih.gov/ij/).

Measurement of Non-Linear Capacitance. Prestin NLC in HEK cells was measured as a function of membrane potential 24 to 48 h after transfection. Cells were bathed in a medium designed to block voltage-dependent ionic currents. The medium consisted of sodium chloride (120.0 mM), magnesium chloride (2.0 mM), tetraethyl ammonium chloride (20.0 mM), cobalt chloride (2.0 mM), dextrose (10.0 mM), and HEPES (10.0 mM), buffered to pH 7.25 and adjusted to 300 mOsm. Cells with clearly membrane-resident fluorescent label were identified on the stage of an Olympus IX-70 inverted microscope (Olympus America, Center Valley, PA) using a 100 magnification 1.4 numerical aperture objective. All electrophysiological measurements were performed at room temperature.

The whole cell patch clamp method was used to measure membrane currents evoked by voltage commands. Patch pipettes were pulled from 8250 glass capillaries (A-M Systems, Carlsborg, WA) on a Sutter P-97 electrode puller (Novato, CA) and polished on a Narashige MF-830 polisher (East Meadow, NY). The pipette solution consisted of cesium chloride (140.0 mM), EGTA (10.0 mM), HEPES (10.0 mM), magnesium chloride (2.0 mM), and potassium adenosine triphosphate (2.0 mM). Filled pipette resistances were between 1.5 and 5.0 MΩ. Membrane currents in response to voltage commands were recorded at the output of a Warner Instruments PC-501A patch clamp amplifier (Hamden, CT). Voltage commands were generated and currents digitized using custom software written in TestPoint (C.E.C. Corp, Burlington, MA) and a Keithley Instruments (KCPI 3801; Cleveland, OH) A/D-D/A board in an IBM PC-type computer. Currents were low-pass filtered at 5 kHz prior to digitization.

The two-sinusoid method (Kakehata and Santos-Sacchi 1996) was used to measure membrane capacitance. This method is superior to other methods, including single-sinusoid methods, because it enables independent calculation of series resistance, which often varies during a stimulus protocol. Simultaneous sinusoidal voltage commands of frequencies 195.3 Hz and 390.6 Hz at amplitudes of 10 mV were superimposed on membrane potential bias commands that were stepped in 32 intervals of 5 mV, starting at -100 mV. The membrane holding potential in the absence of voltage commands was -70 mV. Membrane potentials were corrected off-line for series resistance error but were not corrected for the change in liquid junction potential on breaking into the cell (measured as -4.7 mV). Series resistances were generally less than 20 MΩ. Results were discarded if the cell input resistance were less than 500 MΩ.

Corrected capacitance-membrane potential functions were fitted by the Levenberg-Marquardt algorithm using the program Origin (Origin Lab, Northampton, MA) to the equation:

224
$$C = C_l + \left(\frac{Qz}{kT}\right)\left(\frac{b}{(1+b)^2}\right),$$
$$b = \exp\left(\frac{-ze}{kT}(V - V_{pk})\right)$$

225 (Kakehata and Santos-Sacchi 1996), where C_l is the linear capacitance, V is the membrane
226 potential in volts, V_{pk} is the membrane potential at peak NLC (also in volts), e is the charge on
227 the electron (Coulombs), z is the number of elementary charges transferred by each molecule
228 between states, Q is the total number of elementary charges transferred between states in a cell,
229 and k and T are Boltzmann's constant and absolute temperature, respectively.

230 The results of the curve fits were accepted only if the R^2 goodness of fit value were
231 greater than 0.9 (with one exception, see Results) and the error in any single parameter estimate
232 did not exceed 20% of the estimate. The NLC values were normalized for comparison by
233 dividing by the peak NLC value predicted from the curve fit.

234 *Statistical Analysis of NLC Results.* To prevent potential data discrepancies due to daily
235 fluctuations in equipment and cell passage, mutant NLC measurements were always compared to
236 a similar number of measurements obtained from wild-type transfected cells of the same or
237 similar passage number. Differences in cysteine-mutant and wild-type NLC measurements were
238 analyzed using independent sample t-tests (SPSS, Chicago, IL). The t-tests were corrected for
239 unequal variance when a Levene's Test for Equality of Variance indicated unequal variances
240 between the test and control (wild-type) groups.

241 *Lifetime Imaging of Donor mTFP Fluorescence.* Fixed cells were imaged using a 40x 1.4 n.a. oil
242 immersion objective on the I.B.I.F. confocal microscope. Cells containing donor alone and/or
243 acceptor fluorophore were imaged using a 512 by 512 pixel field with 4x digital magnification.
244 Pre-bleach lifetime images were captured using two-photon excitation at wavelengths of 820 nm

(for cCFP) or 870 nm (for mTFP) with a titanium:sapphire laser (Chameleon Ultra, Coherent Incorporated, Santa Clara, CA) and time-correlated single photon counting (SPC-830, Becker & Hickl, Nahmitzer Damm, Berlin). Donor lifetime was calculated using SPCImaging (Becker & Hickl) with either 1 (mTFP) or 2 (cCFP) decay components (lifetime data range set with minima and maxima of 500 and 3000 ps, and a threshold of 25 photon counts per pixel). The decay matrix distribution over the region of interest was exported. A Gaussian fit of the histogram was calculated using Origin. Cell lifetimes were rejected if the Gaussian fit parameter had a correlation coefficient $R^2 < 0.9$.

FRET Analysis of Oligomerization. The acceptor photobleach fluorescence lifetime imaging version of FRET analysis (apFRET) required five steps: 1) a pre-bleach spectrum determination to determine the relative levels of donor and acceptor fluorescence; 2) a pre-bleach fluorescence lifetime measurement of the acceptor (mTFP or CFP); 3) photobleaching of the acceptor (YFP); 4) a post-bleach fluorescence lifetime measurement of the acceptor; and 5) a post-bleach spectrum determination to determine the effectiveness of the acceptor photobleach. Pre-bleach spectral images were determined using excitation with the 453 nm line of the argon laser of the confocal microscope and were captured using the META detector in lambda mode. Spectral images were linearly un-mixed into either donor or acceptor based on previously-acquired donor and acceptor spectra. If the cell image did not contain approximately equal intensities of donor and acceptor fluorescence, then the image was rejected. Acceptor photobleaching was performed by 30 repetitions of excitation of the region of interest with the 545 nm laser line of the confocal microscope and band-pass filtered from 565 nm to 615 nm. Post-bleach lifetime and spectral images were captured as described above. FRET efficiency was calculated with the following equation:

$$E_{FRET} = \frac{\tau_D - \tau_{DA}}{\tau_D},$$

where E_{FRET} is FRET efficiency, τ_D is the lifetime of donor alone (after photobleaching), and τ_{DA} is the lifetime of the donor in the presence of an acceptor before photobleaching

Results

Determination of Conserved Cysteinyl Residues

More than 110 prestin homologs were identified based on a filtered BLAST database search. Sequences that did not contain both a SulP domain and a STAS domain were not included in the analysis. Homologous sequences were obtained from species in five kingdoms (animals, plants, fungi, amoeba, and bacteria).

We analyzed cysteine conservation by aligning prestin homologs in a subset of sequences (Fig. 1B). Bias towards any phylogeny class was avoided by selecting single Slc26a5 representatives from each chordate class in which a published Slc26a5 homolog exists. The analysis data set included Slc26 sequences from *C. elegans*, *S. purpuratus*, *C. intestinalis*, and *D. discoideum*, as well as non-mammalian and mammalian Slc26a5 ortholog sequences and mammalian (human) sequences of SLC26 paralogs. The phylogenetic relationships between the selected sequences are shown in Fig. 1B, as determined using CLC Main Workbench (see Methods). Particularly noteworthy is the large evolutionary distance between *H. sapiens* SLC26A5 and its paralog SLC26A11, greater even than the distance between mammalian prestin and its *C. intestinalis* and *S. purpuratus* homologs.

We then performed a multiple sequence alignment focused on the cysteinyl residues, also using CLC Main Workbench (Fig. 1C), and organized the results into three groups representing different levels of conservation. The amino-terminal residue C52, which we allocated to Group 1, was identically conserved in all prestin orthologs and nearly all paralogs and homologs. In the only exceptions, human SLC26A7 and *D. discoideum* Sulp, there were gaps at that position, and we also noted poor overall conservation in their amino-terminal sequences. This high degree of

identity conservation suggested a role for C52 in a function common to the entire Slc26 family, such as an ion transport-related function or binding to some membrane-localization element.

The other cysteinyl residues showed mixed patterns of conservation that could be organized in two further groups: those residues that were replaced in paralogs and homologs by mainly polar residues (Group 2) and those that are replaced by mainly non-polar residues (Group 3). Group 2 consisted of C196, C381, and C679. For example, the Group 2 carboxy-terminal residue C679 was identically conserved in all Slc26a5 orthologs and in some closely closely-related paralogs, as determined by the phylogenetic relationships depicted in Fig. 2B. Some paralogs also had a cysteinyl residue in that position (for example, *H. sapiens* SLC26A2), but other polar residues were also found. In the other members of Group 2, the SulP domain residues C196 and C381, the cysteinyl residue was identically conserved in mammalian orthologs (except for the monotreme in C196). In the non-mammalian orthologs, paralogs and homologs, the residue was replaced by one of several small polar residues. The results suggested that Group 2 cysteinyl residues contribute polar character rather than sulfhydryl linkages to structure in the Slc26 family proteins.

The Group 3 cysteinyl residues C126, C192, C415, and C395 (also in the SulP domain) were conserved only in mammalian prestin sequences and were replaced in non-mammalian orthologs, and in paralogs and homologs, with residues of various properties, including polar residues, non-polar aliphatic residues, charged residues, and even prolyl in C260. The most striking of these was C415, which was found to be identically conserved only in the *mammalian* prestin orthologs, which are the ones that have been shown to exhibit large NLC. In the non-mammal orthologs, the paralogs, and the homologs, this cysteinyl residue was replaced by various medium and small hydrophobic residues. This position may therefore be important in

some functional aspect unique to mammalian Slc26a5, such as its membrane-potential-dependent conformation change or the associated NLC. The results of replacement of cysteinyl residues in other paralogs and homologs in Group 3 suggests that neither their polar character nor their ability to form sulfhydryl linkages contribute to conserved, Slc26-related, aspects of prestin structure or function.

We concluded that the cysteinyl residues in Groups 1 and 2 are related to function across the entire Slc26 family, whereas the Group 3 cysteinyl residues more likely contribute to some mammalian prestin-specific function, such as NLC.

All Cysteine-Alanine Substitution Mutations Were Membrane-Targeted

For electrophysiological analysis, we transfected HEK 293 cells with plasmids expressing wild-type prestin or cysteine-substitution prestin mutations as constructs coupled to eGFP. The protein products of wild-type and alanine-substituted prestin-eGFP constructs were synthesized at useful levels within 24 hours of transfection. All appeared to be membrane-targeted. Membrane targeting was confirmed by labeling the membrane of living intact cells with WGA-568, as described in the Methods. Confocal-microscopic observation of labeled cells revealed distinct and nearly-overlapping WGA-568 label and eGFP fluorescence (Fig. 3A). Measurements of label found no significant difference in the relative positions of eGFP and WGA-568 label in all alanine-substitution constructs, indicating incorporation of eGFP-coupled prestin into the plasma membrane (Fig. 3A).

All Cysteine-Alanine Substitution Mutants Were Functional by NLC Analysis

We obtained NLC measurements from transfected and expressing HEK cells using the methods described. All constructs demonstrated NLC, which confirmed our confocal-microscopic analysis of prestin incorporation. NLC results were fitted to Boltzmann-derived functions to

340 determine the NLC parameters, as described in the Methods and Materials section. Plots of
341 averaged normalized NLC values for each of the cysteine-alanine substitution constructs, as a
342 function of membrane potential, are shown in Fig. 4. Functions in this figure were compared to
343 similarly-averaged normalized NLC measurements from cells transfected at about the same time
344 with wild-type prestin.

345 *Four Cysteine-Alanine Substitution Mutations Exhibited Significantly Different NLC to Wild*
346 *Type Prestin*

347 Our statistical analysis of the data is depicted in Fig. 5 and the results listed in Table 1. The
348 analysis showed that the NLC parameters V_{pk} and z were insignificantly different from wild-type
349 NLC in the Group 1 and Group 2 alanine substitutions. However, all of the Group 3 alanine
350 substitutions (with one exception) exhibited significant positive or negative changes in V_{pk},
351 without changes in z.

352 Group 3 cysteinyl residues were replaced in non-mammalian orthologs, paralogs, and
353 homologs by non-polar residues, for the most part. Introducing a non-polar residue (alanine) in
354 place of a cysteinyl had therefore disrupted a function specific to mammalian prestin. We then
355 attempted to determine if the polar nature of the cysteinyl residue, rather than its capacity to form
356 covalent bonds, were functionally significant in NLC. The amino acid serine is closest to
357 cysteine in molecular weight and polar nature. We therefore created cysteinyl-seryl substitutions
358 of prestin-eGFP for the two Group 3 positions with the largest changes in V_{pk} (C124 and C415, >
359 10 mV). Our reasoning for selecting these two positions was that we would have the best chance
360 to detect restoration of normal NLC with recordings from a practical number of cells. We then
361 measured the resulting NLC and compared it to wild-type prestin (Fig. 5 and Table 1). If the

362 polar character of the residue were important, we would expect that the NLC parameters would
363 be restore to wild-type or near wild-type values.

364 For the C124A substitution, V_{pk} was hyperpolarized compared to wild type (-72.78 mV),
365 and z was not significantly different. For the C124S substitution, V_{pk} was also significantly
366 hyperpolarized compared to wild type, although less so than for C124A (-67.65 mV), and z was
367 again not significantly different (Fig. 6A and Table 1). In contrast, for the C415A substitution,
368 V_{pk} was depolarized compared to wild type (-32.11 mV), and z was not significantly different.
369 For the C415S substitution, the substitution of serine essentially corrected the depolarizing effect
370 of alanine substitution at that position (-59.26 mV) (Fig. 6B and Table 1). Thus we conclude that
371 the polar character of the cysteine at position 415 contributes to prestin function.

372 It should be noted that membrane incorporation levels of C415S prestin were remarkably
373 low, although synthesis levels appeared comparable to wild-type prestin. Thus for this construct
374 we resorted to promoting membrane incorporation using incubation with salicylate (see Methods
375 and Materials). Even with this additional step, the fit criterion had to be relaxed to $R^2 > 0.8$ in
376 order to obtain enough measurements.

377 *FRET Efficiency*

378 As explained in the Introduction, oligomerization is a feature of mammalian prestin and at least
379 some paralogs and homologs. We reasoned that if particular cysteinyl residues participate in
380 oligomerization, then wild-type subunits would interact less efficiently with co-transfected
381 alanyl-substituted subunits than with wild-type subunits. We therefore measured FRET
382 efficiency in HEK 293 cells transfected with wild type prestin coupled to the donor (mTFP) and
383 alanine-substituted prestins coupled to the acceptor (vYFP).

First, to establish the limits of our ability to detect FRET using apFRET, we examined several positive and negative controls (Fig 6A). Two positive controls were used: the pLink construct, in which cCFP is ligated in-frame to vYFP; and the pgPT/pgPY combination, in which gerbil prestin donor and acceptor constructs were co-transfected. FRET was detectable with both positive controls, although pLink-transfected cells had significantly greater average FRET efficiencies than cells transfected with the pgPT/pgPY pair (Fig. 6A; Student's t-test, $p < 0.01$).

Several negative controls were also used to establish the minimum detectable FRET efficiency. These included cells transfected with donor alone (pT and pgPT) and cells transfected with a pair not expected to oligomerize (pT/pY and pgPT/p38Y). The average FRET efficiencies obtained for these tests are also shown in Fig 6A. The negative control transfected cells all had significantly smaller average FRET efficiencies than the positive controls (Student's t-test $p < 0.001$), which demonstrated our ability to distinguish between interacting and non-interacting fluorophores. Cells transfected with pgPT had significantly greater FRET efficiencies than the other negative controls (Student's t-test, $p < 0.05$, $p < 0.001$). The other three negative controls were indistinguishable. For the remainder of the FRET experiments, the FRET efficiency of pgPT/pA38Y co-transfected cells was considered the lower level detection of FRET (E_{FRET} = 1.70%) and the FRET efficiency of pgPT/pgPY transfected cells was considered the normal FRET efficiency of gerbil prestin subunits (E_{FRET} = 7.64%).

To test interaction between wild-type and cysteine-substitution mutations, FRET efficiency was measured between wild-type donor subunits and cysteine-mutated acceptor subunit. The average FRET efficiencies are shown in Fig. 7B. All cysteine mutants showed no difference between pgPT/pgPY transfected cells and gPT/cysteine-alanine mutant acceptor construct, except for the cells transfected with pgPT/pgPY-C415A (Dunnett's two-way t-test, $p <$

0.001). The average FRET efficiency of pgPT/pgPY-C415A transfected cells was indistinguishable from the lower limit of FRET detection (Dunnett's one way t-test, $p \geq 0.05$). Thus we concluded that only the Group 3 residue C415 contributes to prestin oligomerization.

Discussion

Our results point to a significant functional role specifically in mammalian prestin for the cysteine at position 415. Mutation of this position to the non-polar amino acid alanine depolarized the peak membrane potential of NLC (V_{pk}) without changing the charge transfer (z). Mutation of the same position to the polar amino acid serine had no effect. Both mutations were functional, in that they underwent the conformation change associated with NLC. This finding, and the preservation of normal function with the serine substitution, eliminates the possibility that the cysteine is required for a sulfhydryl linkage. However, it does not eliminate the possibility that one exists. Indeed, the fact that the alanine substitution reduced or eliminated FRET between it and wild-type prestin suggests a dramatic change in the properties of the assembled molecules. FRET could be reduced by uncoupling of the subunits or by a conformation change that sufficiently separates the carboxy-terminal fluorophores from each other. Our results cannot distinguish between these possibilities. We can, however, assert that the cysteine at position 415 is involved in both NLC and oligomerization in mammalian prestin.

The cysteine at position 415 is one of our Group 3 cysteinyl residues, which are replaced in paralogs and orthologs by a variety of non-polar residues. The Group 3 cysteine residues were predicted, from their lack of conservation, to be involved in mammalian prestin-specific functions, which proved to be the case. For all but one of the Group 3 cysteinyl residues, mutation to alanyl resulted in a change in peak membrane potential of NLC (V_{pk}) (depolarizing for C415, hyperpolarizing for the others) without changing the charge transfer (z). We suggest that these residues contribute to masking (or un-masking) of the voltage sensor governing the prestin conformation change, but do not move during that conformation change, at least not orthogonal to the plane of the membrane.

Mutation of the highly-conserved Group 1 cysteine at position 52 had no effect on NLC. The same applied to the Group 2 cysteinyl residues, which are replaced by polar residues in non-mammalian prestin, and in paralogs and homologs. The Group 2 cysteinyl residues are not apparently required to form sulfhydryl linkages for functionally normal mammalian prestin, although as before we cannot dismiss the possibility that they are present. Nor are they required for oligomerization. They may participate in hydrogen bonding, as may their polar substitutes in other Slc26 family members, but if so it may contribute to some family-wide function such as ion transport or binding to membrane-localization elements.

All of the Group 3 cysteinyl residues, with the exception of C395, appear to participate in NLC to some degree, since the substitution of alanyl modified V_{pk}, without however modifying z. Modifying V_{pk} alone suggests an effect on the voltage sensor, without modification of the conformation change, or at least that part of the conformation change that contributes to NLC. The cysteinyl may be masking, or unmasking, the voltage sensor to some extent. Current hypotheses attribute the NLC to either movement of a bound chloride ion (like a transporter) or movement of charged or polar residues, modulated by chloride ions in an allosteric manner (D. Oliver et al., 2001; V. Rybalchenko and J. Santos-Sacchi, 2003). If the bound chloride hypothesis applies, we might infer that the affinity of prestin for the chloride ion had been modified by alanyl substitution, but the translocation of chloride was unaltered. If the allosteric modulation hypothesis applies, we might infer that either the chloride binding site, or the voltage sensor, had been modified by alanyl substitution. Without further information, it is not yet possible to distinguish between these hypotheses.

455 We do not find the apparent hyperpolarized shift in V_{pk} in wild-type prestin relative to
456 isolated hair cells (Bai et al. 2010; McGuire et al. 2010). Our average V_{pk} for wild-type prestin, -
457 51 mV, is much closer to reported V_{pk} values for OHCs and prestin-transfected HEK cells.
458 The percentage FRET obtained with pgPT/pgPY, at 7%, is substantial and comparable to
459 recent observations by us and other laboratories (McGuire et al. 2010; Navaratnam et al. 2005;
460 Wu et al. 2007). The higher FRET percentage of the pLink construct (20%) is likely a
461 consequence of the forced 1:1 donor:acceptor ratio and the short distance between the donor and
462 acceptor fluorophores in the construct. The higher FRET efficiency of gPT alone may be due to
463 donor-to-donor FRET (Koushik and Vogel 2008) in the dense puncta of fluorescent label that are
464 normally seen in HEK cells ((Rajagopalan et al. 2007) and our own observations).
465 We have chosen not to report Q/C_l results as a measure of membrane incorporation, as
466 others have done (Bai et al. 2010; McGuire et al. 2010), because they do not have the
467 significance ascribed to them. In transfected cell experiments, the cells selected for examination
468 are a vanishingly small subset of those available to the experimenter, and are undoubtedly
469 selected to be those with the clearest membrane label. Even then, the experimenter does not
470 sample a fixed number of cells but continues until a satisfactory number of recordings has been
471 achieved. Thus the sample population is far from unbiased. Further, C_l is a poor predictor of Q
472 even for a single construct. In our analysis of 107 cells that were visibly synthesizing wild-type
473 prestin (coupled to eGFP) and incorporating it into their membranes, Q was only weakly
474 correlated with C_l (Fig. 8). We conclude that comparisons of membrane incorporation between
475 mutations using Q/C_l are not reliable. This is not to say that there are no differences among
476 constructs in membrane incorporation. For example, as we describe, the C415S construct was

robustly synthesized but poorly incorporated into the membrane, so much so that a frustratingly large number of cells had to be examined to provide even the limited data shown here.

Acknowledgments

We acknowledge the use of the confocal microscope facility of the Integrated Biomedical Imaging Facility of Creighton University. We thank Dr. Atsushi Miyawaki (RIKEN Brain Science Institute, Japan), Dr. Jian Zuo (St. Jude Children's Research Hospital, Memphis, TN), and Dr. Peter Dallos (Northwestern University, Evanston, IL) for gifts of cDNA. We thank Dr. Jing Zheng and Dr. Peter Dallos of Northwestern University, and Dr. Kirk Beisel and Dr. Venkatesh Govindarajan of Creighton University, for valued help in getting these experiments started. Present address of Benjamin Currall: Department of Pathology, Brigham and Women's Hospital, Harvard Medical School.

Grants

Supported by N.S.F.-Nebraska EPSCoR EPS-0701892 to R.H. Research was conducted in a facility constructed with support from Research Facilities Improvement Program C06 RR17417-01 from the National Center for Research Resources (N.C.R.R.) of the National Institutes of Health (N.I.H.). The Integrated Biomedical Imaging Facility is supported in part by grant P20 RR16469 from the N.C.R.R., N.I.H.

Disclosures

The authors disclose no conflicts of interest.

References

Bai JP, Surguchev A, Bian S, Song L, Santos-Sacchi J, and Navaratnam D. Combinatorial cysteine mutagenesis reveals a critical intramonomer role for cysteines in prestin voltage sensing. *Biophys J* 99: 85-94, 2010.

Dallos P. Cochlear amplification, outer hair cells and prestin. *Curr Opin Neurobiol* 18: 370-376, 2008.

Dallos P, Wu X, Cheatham MA, Gao J, Zheng J, Anderson CT, Jia S, Wang X, Cheng WH, Sengupta S, He DZ, and Zuo J. Prestin-based outer hair cell motility is necessary for mammalian cochlear amplification. *Neuron* 58: 333-339, 2008.

Day RN, Booker CF, and Periasamy A. Characterization of an improved donor fluorescent protein for Forster resonance energy transfer microscopy. *J Biomed Opt* 13: 031203, 2008.

Detro-Dassen S, Schanzler M, Lauks H, Martin I, zu Berstenhorst SM, Nothmann D, Torres-Salazar D, Hidalgo P, Schmalzing G, and Fahlke C. Conserved dimeric subunit stoichiometry of SLC26 multifunctional anion exchangers. *J Biol Chem* 283: 4177-4188, 2008.

Dorwart MR, Shcheynikov N, Yang D, and Muallem S. The solute carrier 26 family of proteins in epithelial ion transport. *Physiology (Bethesda)* 23: 104-114, 2008.

Feng DF, and Doolittle RF. Progressive sequence alignment as a prerequisite to correct phylogenetic trees. *J Mol Evol* 25: 351-360, 1987.

Greeson JN, Organ LE, Pereira FA, and Raphael RM. Assessment of prestin self-association using fluorescence resonance energy transfer. *Brain Res* 2006.

Iwasa KH. Effect of stress on the membrane capacitance of the auditory outer hair cell. *Biophys J* 65: 492-498, 1993.

Kakehata S, and Santos-Sacchi J. Effects of salicylate and lanthanides on outer hair cell motility and associated gating charge. *J Neurosci* 16: 4881-4889, 1996.

Kakehata S, and Santos-Sacchi J. Membrane tension directly shifts voltage dependence of outer hair cell motility and associated gating charge. *Biophys J* 68: 2190-2197, 1995.

Koushik SV, and Vogel SS. Energy migration alters the fluorescence lifetime of Cerulean: implications for fluorescence lifetime imaging Forster resonance energy transfer measurements. *J Biomed Opt* 13: 031204, 2008.

Kumano S, Iida K, Ishihara K, Murakoshi M, Tsumoto K, Ikeda K, Kumagai I, Kobayashi T, and Wada H. Salicylate-induced translocation of prestin having mutation in the GTSRH sequence to the plasma membrane. *FEBS Lett* 584: 2327-2332, 2010.

Liberman MC, Gao J, He DZ, Wu X, Jia S, and Zuo J. Prestin is required for electromotility of the outer hair cell and for the cochlear amplifier. *Nature* 419: 300-304, 2002.

Ludwig J, Oliver D, Frank G, Klocker N, Gummer AW, and Fakler B. Reciprocal electromechanical properties of rat prestin: the motor molecule from rat outer hair cells. *Proc Natl Acad Sci U S A* 98: 4178-4183, 2001.

McGuire RM, Liu H, Pereira FA, and Raphael RM. Cysteine mutagenesis reveals transmembrane residues associated with charge translocation in prestin. *J Biol Chem* 285: 3103-3113, 2010.

Nagai T, Ibata K, Park ES, Kubota M, Mikoshiba K, and Miyawaki A. A variant of yellow fluorescent protein with fast and efficient maturation for cell-biological applications. *Nat Biotechnol* 20: 87-90, 2002.

Navaratnam D, Bai JP, Samaranayake H, and Santos-Sacchi J. N-terminal-mediated homomultimerization of prestin, the outer hair cell motor protein. *Biophys J* 89: 3345-3352, 2005.

Ohana E, Yang D, Shcheynikov N, and Muallem S. Diverse transport modes by the solute carrier 26 family of anion transporters. *J Physiol* 587: 2179-2185, 2009.

Okoruwa OE, Weston MD, Sanjeevi DC, Millemon AR, Fritzsch B, Hallworth R, and Beisel KW. Evolutionary insights into the unique electromotility motor of mammalian outer hair cells. *Evol Dev* 10: 300-315, 2008.

Oliver D, He DZ, Klocker N, Ludwig J, Schulte U, Waldegger S, Ruppersberg JP, Dallos P, and Fakler B. Intracellular anions as the voltage sensor of prestin, the outer hair cell motor protein. *Science* 292: 2340-2343, 2001.

Rajagopalan L, Greeson JN, Xia A, Liu H, Sturm A, Raphael RM, Davidson AL, Oghalai JS, Pereira FA, and Brownell WE. Tuning of the outer hair cell motor by membrane cholesterol. *J Biol Chem* 282: 36659-36670, 2007.

protein. *Science* 292:2340-2343, 2001.

Rybalchenko V, Santos-Sacchi J. Cl- flux through a non-selective, stretch-sensitive conductance influences the outer hair cell motor of the guinea-pig. *J Physiol* 547:873-891, 2003.

Santos-Sacchi J. Reversible inhibition of voltage-dependent outer hair cell motility and capacitance. *J Neurosci* 11: 3096-3110, 1991.

Schaechinger TJ, and Oliver D. Nonmammalian orthologs of prestin (SLC26A5) are electrogenic divalent/chloride anion exchangers. *Proc Natl Acad Sci U S A* 104: 7693-7698, 2007.

Suhling K, French PM, and Phillips D. Time-resolved fluorescence microscopy. *Photochem Photobiol Sci* 4: 13-22, 2005.

Tan X, Pecka JL, Tang J, Okoruwa OE, Zhang Q, Beisel KW, and He DZ. From zebrafish to mammal: functional evolution of prestin, the motor protein of cochlear outer hair cells. *J Neurophysiol* 105: 36-44, 2010.

Tunstall MJ, Gale JE, and Ashmore JF. Action of salicylate on membrane capacitance of outer hair cells from the guinea-pig cochlea. *J Physiol* 485 (Pt 3): 739-752, 1995.

Wu X, Currall B, Yamashita T, Parker LL, Hallworth R, and Zuo J. Prestin-prestin and prestin-GLUT5 interactions in HEK293T cells. *Dev Neurobiol* 67: 483-497, 2007.

Zheng J, Du GG, Anderson CT, Keller JP, Orem A, Dallos P, and Cheatham M. Analysis of the oligomeric structure of the motor protein prestin. *J Biol Chem* 281: 19916 - 19924, 2006.

Zheng J, Shen W, He DZ, Long KB, Madison LD, and Dallos P. Prestin is the motor protein of cochlear outer hair cells. *Nature* 405: 149-155, 2000.

583 **Figures**

584 Figure 1. Homology analysis of prestin. (A) Region, domain, and motif designation of the human
585 prestin amino acid sequence; green – trans-membrane region, blue – SulP domain, red – STAS
586 domain, and yellow – SulP motif. (B) Phylogeny of SulP family member proteins; number at
587 each node – bootstrap number out of 100 repetitions. (C) Multiple sequence alignment of
588 cysteinyl residues; residue properties: grey – small size hydrophobic, green – medium size
589 hydrophobic, cyan – partial positive charge, blue – positive charge, orange - partial negative
590 charge, red – negative charge, pink – proline, light purple – histidine, and yellow – special
591 property.

592 Figure 2. Diagram showing the positions of the nine cysteinyl residues in prestin, represented by
593 small grey disks, in the two proposed membrane topologies. Above, based on Zheng et al.
594 (2006). Below, based on Navaratnam et al. (2005).

595 Figure 3. Determination of successful membrane targeting of prestin mutations. A) Typical HEK
596 cell expressing prestin-eGFP (green) and labeled with WGA-633 (red). Inset – fluorescence
597 intensity profiles of the line in the main figure. B) Average (and one s.e.m.) of separation of
598 WGA-633 and prestin in profiles, as in A) for wild type and mutated prestins as indicated.

599 Figure 4. Normalized NLC as a function of membrane potential for cysteine-alanine substitutions
600 (filled symbols) compared to wild-type prestin (open symbols). Functions are not corrected for
601 series resistance membrane potential error, which, though small (0.4% or less), means that the
602 plots are shown for illustrative purposes only.

603 Figure 5. Summary of NLC properties of cysteine-alanine substitutions (filled symbols)
604 compared to wild-type prestin (open symbols), plotted as mean plus 1 s.e.m. A) V_{pk}. B) z. Open

star indicates different from wild type at $p < 0.05$, filled star indicates different from wild type at $p < 0.001$.

Figure 6. A) Normalized NLC of C124A (filled symbols), C124S (grey symbols), and wild-type prestin (open symbols) as a function of membrane potential. B) Normalized NLC of C415A (filled symbols), C415S (grey symbols), and wild-type prestin (open symbols), as a function of membrane potential. Functions are not corrected for series resistance membrane potential error.

Figure 7. Averaged FRET efficiencies of control and prestin construct-transfected cells. (A) FRET efficiencies of cells transfected with negative controls (left) or positive controls (right); negative control ANOVA (3, 108, $p < 0.01$) and Student's t-tests. * indicates $p < 0.05$. *** indicates $p < 0.001$. (B) Comparison of FRET efficiencies of positive (left) or negative control (dashed line) to wild-type/mutant donor/acceptor co-transfected cells (right); ANOVA against positive control (9, 320, $p < 0.001$), ANOVA against negative control (9, 295, $p < 0.001$), and Dunnett's two sided t-tests. *** indicates $p < 0.001$. Error bars equal to one SEM.

Figure 8. Total non-linear charge transfer as a function of linear capacitance for 117 cells synthesizing wild-type prestin (slope = 0.0058 pC/pF, $R = 0.118$).

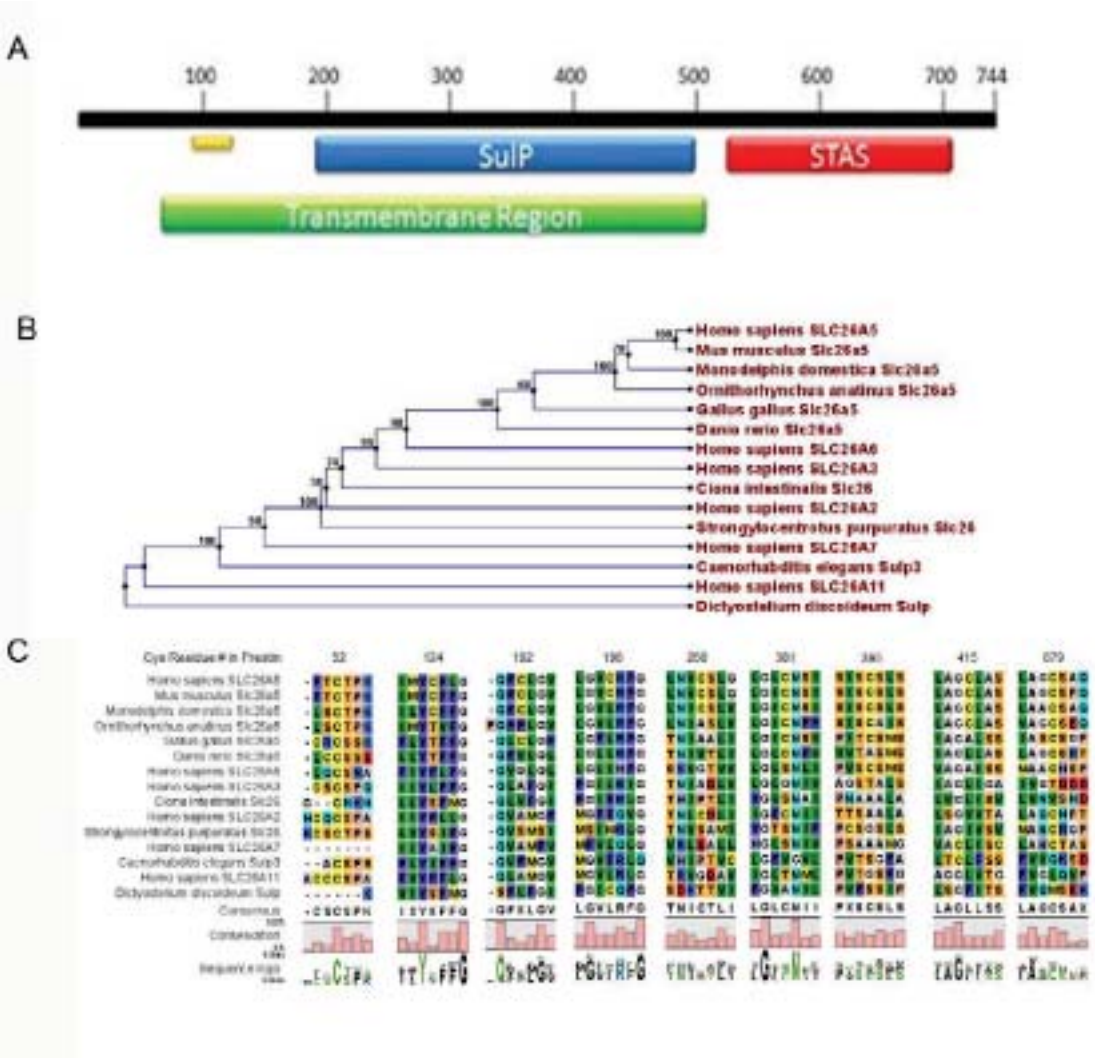
A
100
200
300
400
500
600
700
744
SulP
STAS
Transmembrane Region
B
Homo sapiens SLC26A5
Mus musculus Slc26a5
Monodelphis domestica Slc26a5
Ornithorhynchus anatinus Slc26a5
Gallus gallus Slc26a5
Danio rerio Slc26a5
Homo sapiens SLC26A6
Homo sapiens SLC26A3
Ciona intestinalis Slc26
Homo sapiens SLC26A2
Strongylocentrotus purpuratus Slc26
Homo sapiens SLC26A7
Caenorhabditis elegans Sulp3
Homo sapiens SLC26A11
Dictyostelium discoideum Sulp
C

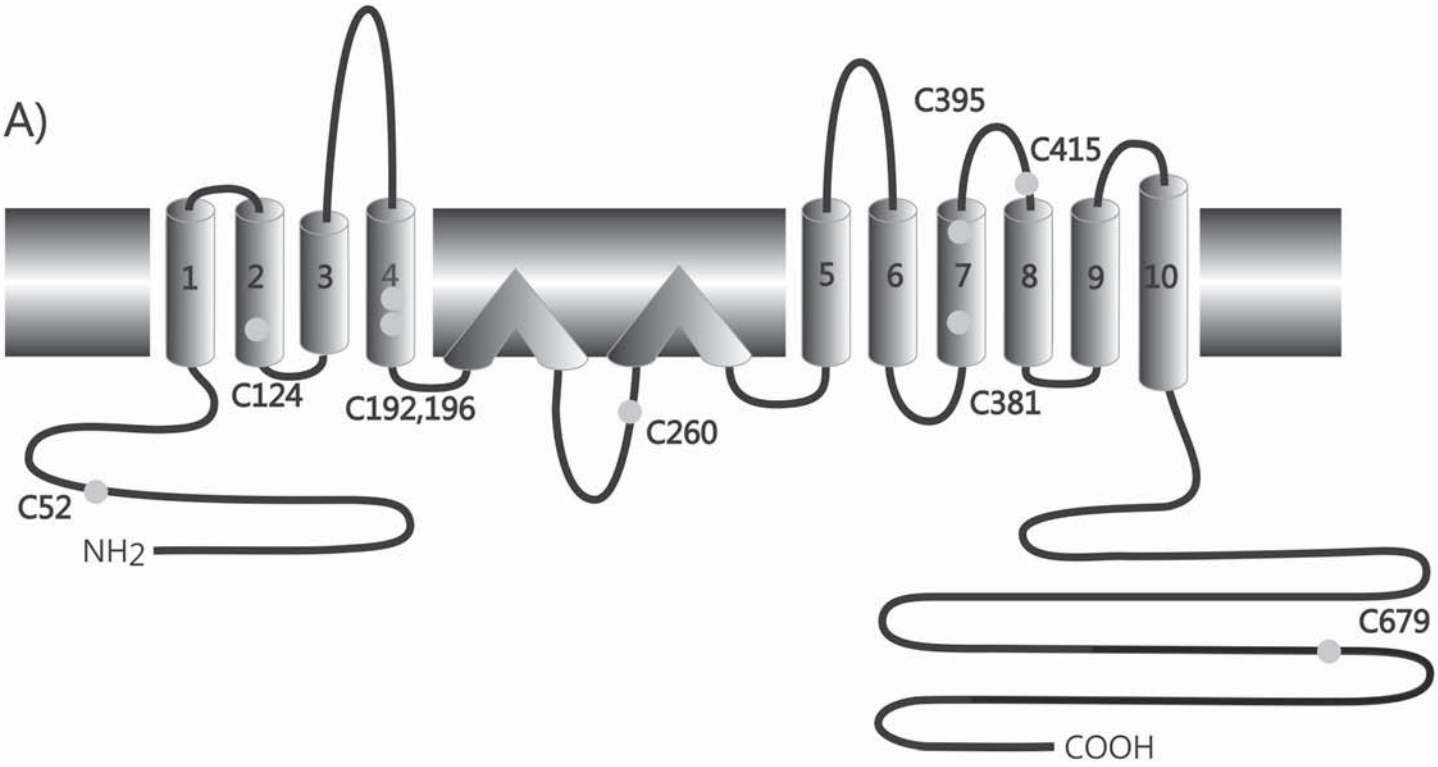
A)
C395
C415
1
2
3
4
5
6
7
8
9
10
C124
C192,196
C260
C381
C52
NH2
C679
COOH

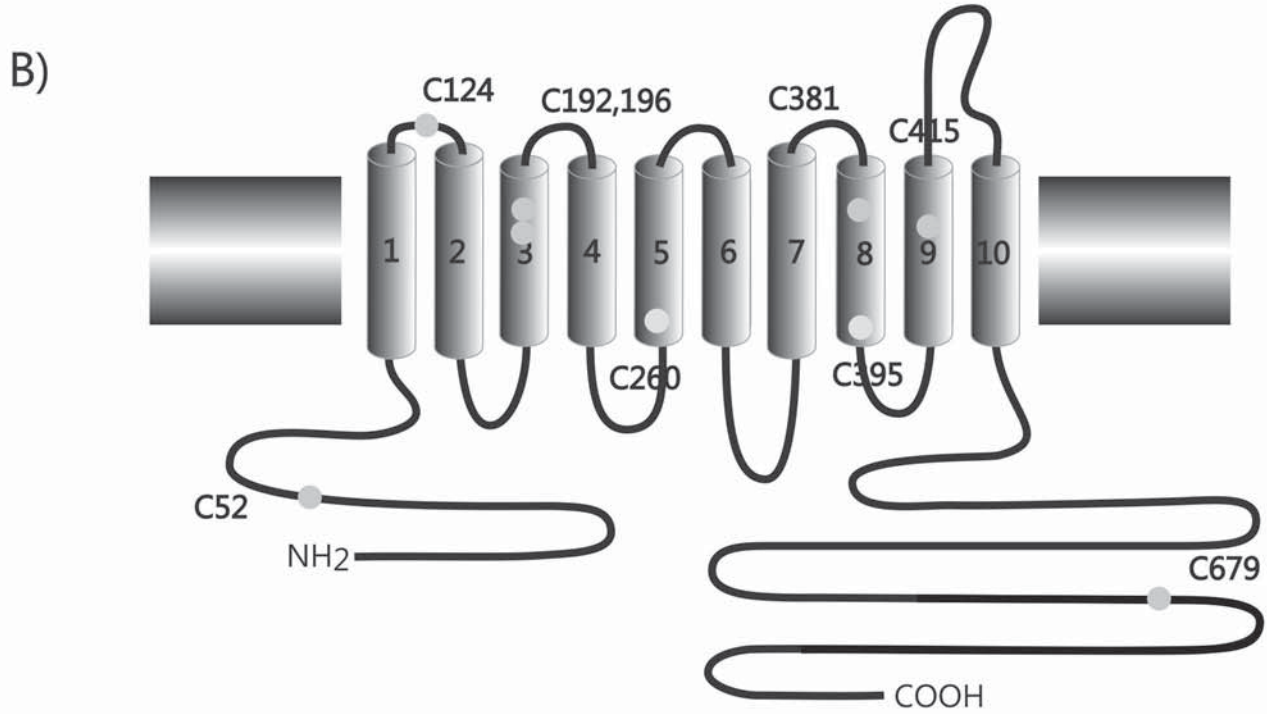
B)
C124
C192,196
C381
C415
1
2
3
4
5
6
7
8
9
10
C260
C395
C52
NH2
C679
COOH

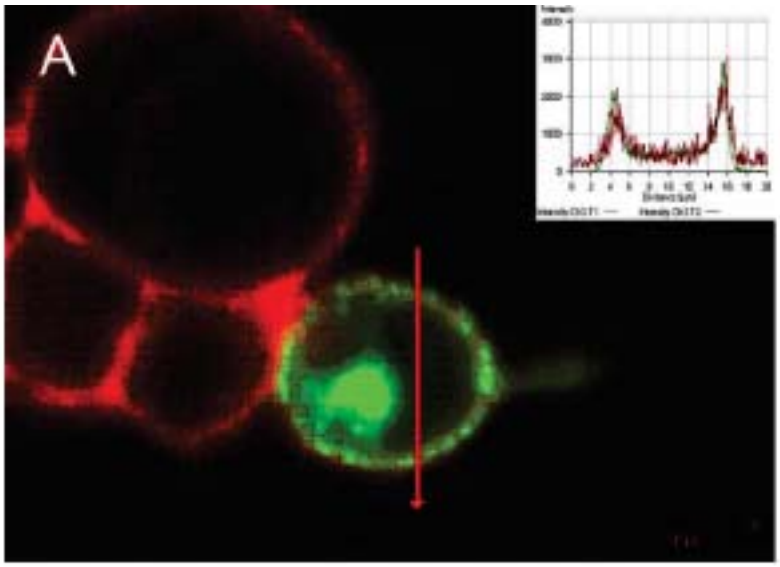
A

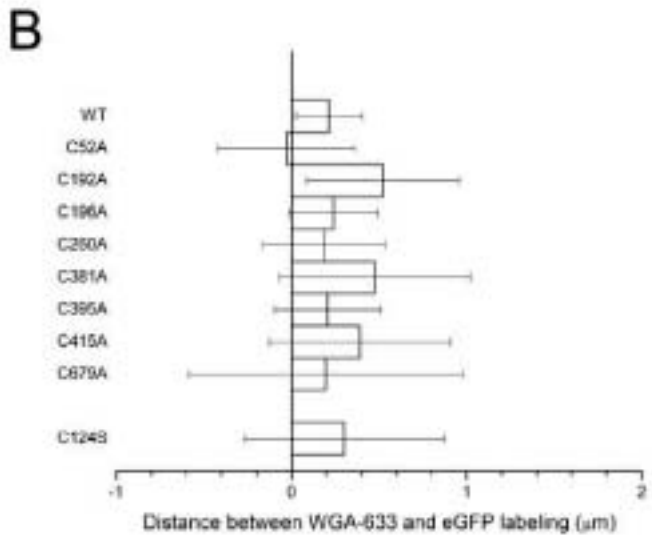
B
WT
C52A
C192A
C196A
C250A
C381A
C395A
C415A
C679A
C124S
-1
0
1
2
Distance between WGA-633 and eGFP labeling (μm)

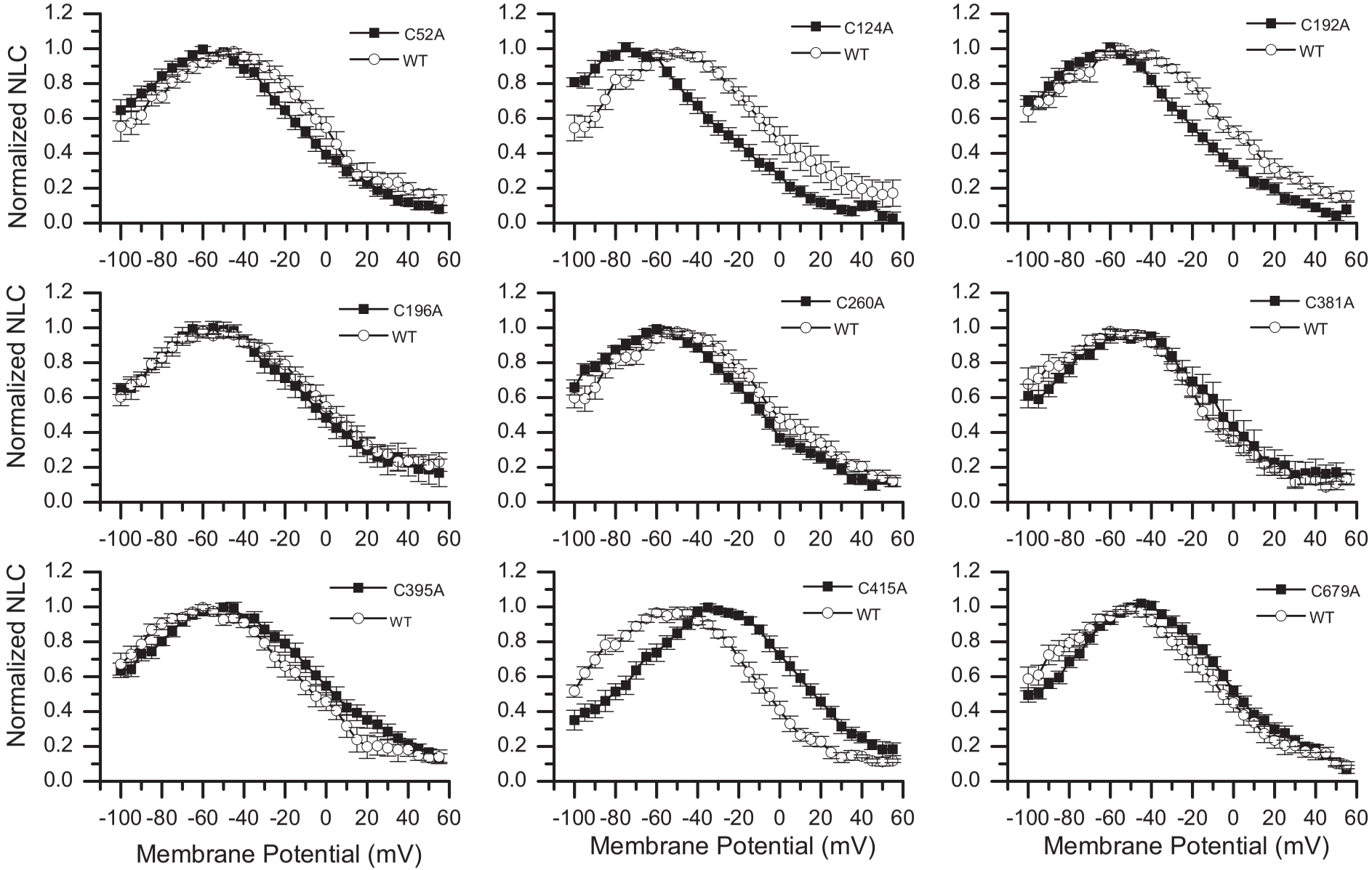
Normalized NLC
Membrane Potential (mV)
C52A
WT
C124A
WT
C192A
WT
C196A
WT
C260A
WT
C381A
WT
C395A
WT
C415A
WT
C679A
WT

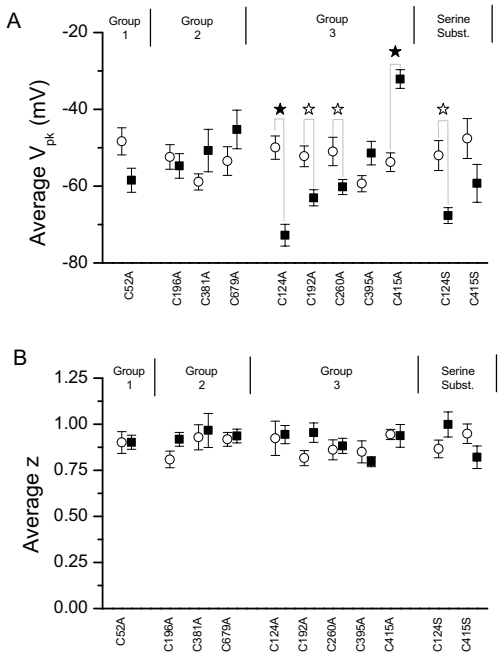
A
Group 1
Group 2
Group 3
Serine Subst.
Average V_{pk} (mV)
-20
-40
-60
-80
C52A
C196A
C381A
C679A
C124A
C192A
C260A
C395A
C415A
C124S
C415S
B
Group 1
Group 2
Group 3
Serine Subst.
Average z
1.25
1.00
0.75
0.50
0.25
0.00
C52A
C196A
C381A
C679A
C124A
C192A
C260A
C395A
C415A
C124S
C415S

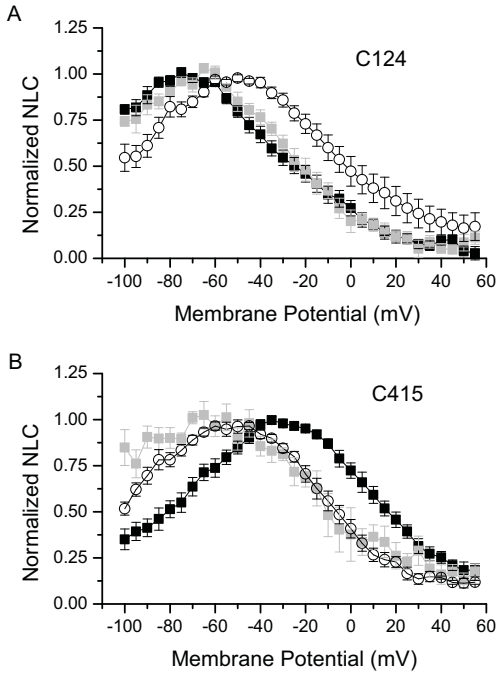
A
C124
Normalized NLC
1.25
1.00
0.75
0.50
0.25
0.00
-100 -80 -60 -40 -20 0 20 40 60
Membrane Potential (mV)
B
C415
Normalized NLC
1.25
1.00
0.75
0.50
0.25
0.00
-100 -80 -60 -40 -20 0 20 40 60
Membrane Potential (mV)

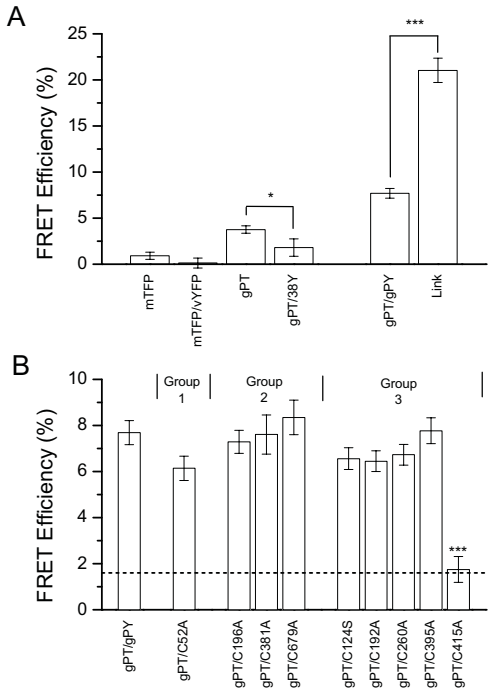
A
FRET Efficiency (%)
25
20
15
10
5
0
***
*
mTFP
mTFP/vYFP
gPT
gPT/38Y
gPT/gPY
Link
B
FRET Efficiency (%)
10
8
6
4
2
0
Group 1
Group 2
Group 3
***
gPT/gPY
gPT/C52A
gPT/C196A
gPT/C381A
gPT/C679A
gPT/C124S
gPT/C192A
gPT/C260A
gPT/C395A
gPT/C415A

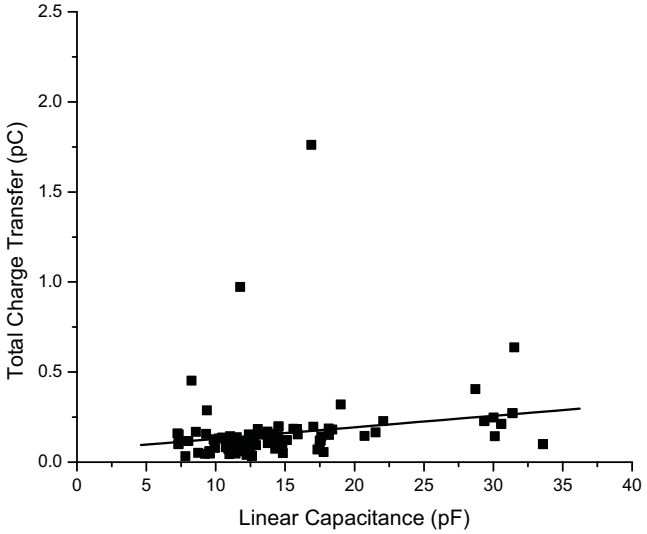
Total Charge Transfer (pC)
Linear Capacitance (pF)
0.0
0.5
1.0
1.5
2.0
2.5
0
5
10
15
20
25
30
35
40

Table 1: Averaged V_{pk} and z of prestin NLC of wild-type prestin and the prestin mutation in this study, and their statistical significance differences to the wild type in the same batch, and their conservation group status.

Conserved	*Mutation*		V_{pk} *(mV)*		*p*	*z*		*p*
Group 1	C52A	*Control*	-48.33			0.901		
		Test		-58.45	*0.051*		0.902	*0.986*
Group 2	C196A	*Control*	-52.38			0.809		
		Test		-54.71			0.918	*0.082*
	C381A	*Control*	-50.25			0.913		
		Test		-59.34	*0.211*		0.931	*0.907*
	C679A	*Control*	-53.48			0.918		
		Test		-45.25	*0.055*		0.936	*0.740*
Group 3	C124A	*Control*	-49.94			0.923		
		Test		-72.78	*<0.001*		0.944	*0.849*
	C192A	*Control*	-52.23			0.817		
		Test		-63.05	*0.006*		0.954	*0.077*
	C260A	*Control*	-50.98			0.861		
		Test		-60.22	*0.025*		0.882	*0.766*
	C395A	*Control*	-59.34			0.850		
		Test		-51.41	*0.053*		0.797	*0.438*
	C415A	*Control*	-53.74			0.944		
		Test		-32.11	*<0.001*		0.937	*0.928*
Group 3	C124S	*Control*	-52.03			0.866		
		Test		-67.65	*0.007*		0.997	*0.124*
	C415S	*Control*	-47.62			0.949		
		Test		-59.26	*0.132*		0.821	*0.139*